OL Organic Letters

pubs.acs.org/OrgLett Letter

Photocatalytic Aminative Suzuki–Miyaura C(sp^2)–N–C(sp^3) Cross-Coupling

Fujun Li, Yun Zou, Shuyang Liu, Yiming Xu, Yunhe Jin,* and Shengyang Tao*

Cite This: *Org. Lett.* 2025, 27, 8823–8828 Read Online

ACCESS | Metrics & More | Article Recommendations | Supporting Information

ABSTRACT: This study introduces a photoinduced Suzuki–Miyaura C(sp^2)–C(sp^3) coupling protocol in which the introduction of a nitrene reagent efficiently redirects the conventional C(sp^2)–C(sp^3) linkage toward a C(sp^2)–N–C(sp^3)-bridged architecture. A total of 432 reactions were conducted using a high-throughput screening strategy to identify the optimal parameters. This strategy exhibits mild conditions, convenient operation, and good functional group tolerance, meanwhile establishing a solid foundation for further developing novel catalytic systems of cross-coupling reactions.

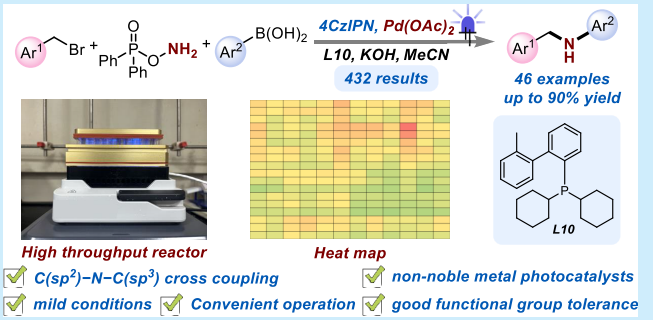

Transition-metal-catalyzed cross-coupling reactions have evolved into one of the most indispensable tools in modern organic synthesis,[1] finding widespread applications in the development of pharmaceuticals, natural products, agrochemicals, energy storage materials, and functional polymers.[2] Among the various strategies, Suzuki–Miyaura and Buchwald–Hartwig couplings represent two of the most prominent pathways for the formation of C–C[3] and C–N[4] bonds, respectively. Although traditional cross-coupling methodologies have substantially expanded the synthetic repertoire of organic chemistry, continued progress in the field has fueled the pursuit of innovative approaches to transcend the inherent limitations of classical protocols and to enable access to increasingly diverse and architecturally complex molecular frameworks.[5] To overcome the limitations of conventional two-component couplings, the strategic insertion or deletion of intermediate components has been introduced to enable novel bond-forming paradigms.[6] A recent study by Liu and coworkers reported an innovative three-component coupling strategy, in which nitrene insertion was incorporated into the palladium-catalyzed Suzuki–Miyaura C(sp^2)–C(sp^2) cross-coupling pathway, successfully transforming the C(sp^2)–C(sp^2) bond into a C(sp^2)–N–C(sp^2) linkage (Scheme 1a, top half).[7] However, applying this aminative strategy to C(sp^3)–C(sp^2) cross-couplings remains challenging due to the hard oxidative insertion of C(sp^3)–X bonds into metal centers suffering from reaction efficiency and poor regioselectivity.[8] These issues are likely attributed to the involvement of two-electron oxidative addition pathways in such systems along with the propensity of alkylmetal intermediates to undergo β-hydride elimination and associated isomerization processes.

Scheme 1. Aminative Suzuki–Miyaura Cross-Coupling

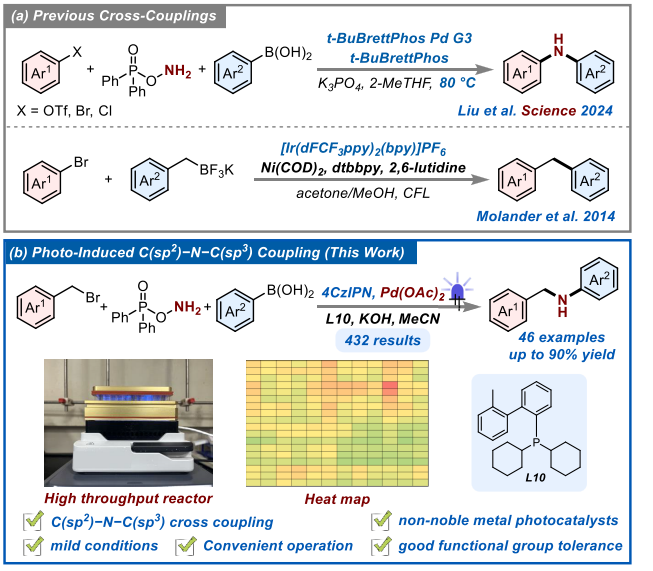

Photocatalytic methodologies have emerged as an innovative paradigm in sustainable synthesis,[9] enabling open-shell-mediated bond formation with enhanced environmental

Received: May 22, 2025
Revised: July 29, 2025
Accepted: August 4, 2025
Published: August 6, 2025

https://doi.org/10.1021/acs.orglett.5c02073
Org. Lett. 2025, 27, 8823–8828

compatibility. Among them, dual catalysis approaches leverage single-electron transfer (SET) events mediated by photoexcited catalysts, effectively circumventing conventional transition-metal-catalyzed two-electron oxidative addition pathways through radical intermediates and thereby demonstrating unique reaction advantages.[10] In 2014, the Molander group pioneered a mechanistically distinct SET strategy using an iridium photoredox catalyst with a nickel catalyst to activate organoboron reagents and promote transmetalation (Scheme 1a, bottom half).[11] This method enables the cross-coupling of alkoxyalkyl or benzyl trifluoroborate salts with a broad range of aryl bromides under exceptionally mild conditions. Nevertheless, the inherent complexity of such multicomponent catalytic systems requiring precise coordination among the photocatalyst, transition metal catalyst, ligand, and base presents an increasing workload in reaction optimization. High-throughput experimentation (HTE) is widely recognized in synthetic chemistry as a powerful tool that significantly accelerates data acquisition and thereby empowers more efficient exploration.[12]

Based on the above issues and our research experience on photocatalysis,[13] we herein employed HTE to rapidly identify the optimal reaction combinatorially. Under photoirradiation and ambient conditions, a nitrene species was successfully inserted into the Suzuki $C(sp^2)-C(sp^3)$ cross-coupling pathway, enabling a directed transformation from $C(sp^2)-C(sp^3)$ to $C(sp^2)-N-C(sp^3)$ linkages (Scheme 1b). This strategy provides a concise route to $C(sp^2)-N-C(sp^3)$ motifs and offers a practical tool for amine insertion in fine chemical synthesis.

Initially, we performed a preliminary screening of reaction conditions with 4-trifluoromethylbenzyl bromide **1a** and 2-methylphenylboronic acid **1c** used as template reactions, acquiring a 20% yield for $C(sp^2)-N-C(sp^3)$ products along with a 35% yield for $C(sp^2)-C(sp^3)$ products (for details, see Table S1). Building on this foundation, a HTE campaign was conducted, encompassing 3 solvents, 6 bases, 2 palladium catalysts, and 12 ligands, resulting in a total of 432 distinct reaction conditions (for details, see Table S2 and Figures S2–S6). Using product yields as the evaluation metric, data visualization was employed to intuitively reveal reaction trends, with the experimental results summarized as heat maps in Figure 1. Specifically, Figure 1b and c illustrates the influence of various reaction conditions on product yields when using *t*BuBrettPhos PdG3 and $Pd(OAc)_2$ as catalysts, respectively.

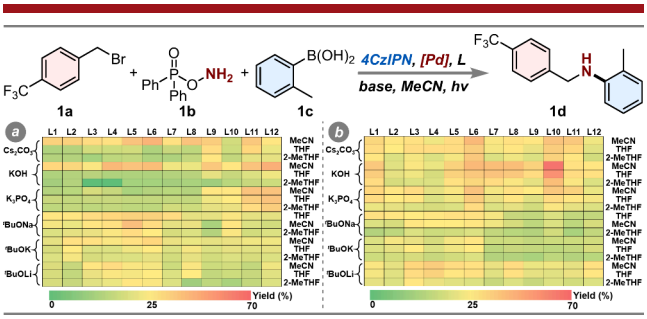

Figure 1. Visualized heatmaps. (a) Experimental results for *t*BuBrettPhos PdG3. (b) Experimental results for $Pd(OAc)_2$. Reaction conditions: **1a** (0.05 mmol), **1b** (0.08 mmol), **1c** (0.1 mmol), 4CzIPN (1 mol %), [Pd] (3 mol %), ligand (5 mol %), base (3 equiv), sovent (520 μL), N_2, rt, 365 nm, 45 mW, and 20 h, with the HPLC yield (external standard).

Systematic analysis of the heat map revealed that, under identical reaction conditions, the $Pd(OAc)_2$ catalytic system generally afforded higher yields compared to the *t*BuBrettPhos PdG3 system. Among the tested ligands, **L10** delivered the highest yield (65%) within the $Pd(OAc)_2$ catalytic framework. Moreover, in terms of the solvent effect, the yields obtained when MeCN was used as a solvent were significantly higher than those provided with THF or 2-MeTHF, keeping all other conditions constant. Besides, KOH demonstrated optimal efficacy in the screening of the base. In the meantime, it was shown by high-throughput experiments that the method has good reproducibility (for details, see Table S3). The combined analysis gave a yield of 65% under the following conditions: catalyst, $Pd(OAc)_2$; solvent, MeCN; base, KOH; and ligand, **L10**.

Based on the above experimental conditions, we further explored the optimization of each reaction parameter. Under reaction conditions of 0.09 equiv of $Pd(OAc)_2$, 2.5 equiv of KOH, 1.6 equiv of **1b**, and 45 mW irradiation for 20 h, the target product **1d** was obtained with a yield of 75%, along with 20% Suzuki-type byproduct **1e**. Additionally, under these optimized conditions, we evaluated the scalability of the reaction by transitioning from the microscale high-throughput format (entry 1) to a preparative-scale reaction (entry 10), also yielding a competitive result (for details, see Table S4). Under optimal conditions, screening amine sources improved yields, while the highest yield was still with **1b** (for details, see Table S5).

After the optimal conditions were established, the substrate scope was extended. As shown in Scheme 2, unsubstituted benzyl bromide (**2d**) underwent the reaction smoothly under the optimized conditions, delivering a slightly improved yield of 80%. Electron-donating alkyl groups, such as methyl, isopropyl, and *tert*-butyl (**3d**–**5d**), afforded yields of 73–86%, showing a slight increase with stronger donation. The substituent position and number (**6d**–**9d**) had little effect, with yields remaining between 75 and 83%. Fortunately, strong electron-donating groups (**10d**–**12d**) were further introduced, leading to increased yields of up to 90%. In contrast, electron-withdrawing groups (e.g., halogen, ester, and cyano; **13d**–**18d**) led to reduced yields (40–78%), decreasing with an increasing electron-withdrawing strength. Notably, the substrate bearing both electron-donating and -withdrawing groups (**19d**) was obtained in 73% yield, likely due to electronic compensation. Polycyclic aromatics (**20d** and **21d**) also reacted smoothly, affording 65 and 84% yields, respectively.

In the extension to arylboronic acid substrates, unsubstituted phenylboronic acid (**22d**) was smoothly converted to a yield of 75%. Introducing various *para*-alkyl substituents (**23d**–**27d**) maintained high yields (68–82%), indicating the minimal impact of these groups on the reaction efficiency. Migrating these substitutions to *ortho* or *meta* positions (**28d**–**30d**) was also tolerated, giving 70–78% yields. Polyalkyl variants (**31d** and **32d**) reacted comparably (70 and 76%) as well. Furthermore, introducing methoxy groups at the *ortho* or *para* positions (**33d** and **34d**) boosted efficiency to 90%, whereas replacement with phenoxy (**35d**) lowered the yield to 65%. Incorporation of strong electron-withdrawing substituents (**36d**–**38d**) on the aryl ring irrespective of *ortho* or *meta* sites markedly attenuated reactivity, with yields falling to around 55%. By contrast, more complex frameworks, such as naphthyl and benzofuran (**39d**–**41d**), were readily accommodated, furnishing 65–82% yields. Heterocyclic substrates,

https://doi.org/10.1021/acs.orglett.5c02073
Org. Lett. 2025, 27, 8823–8828

Scheme 2. Reaction Substrate Applicability[a,b]

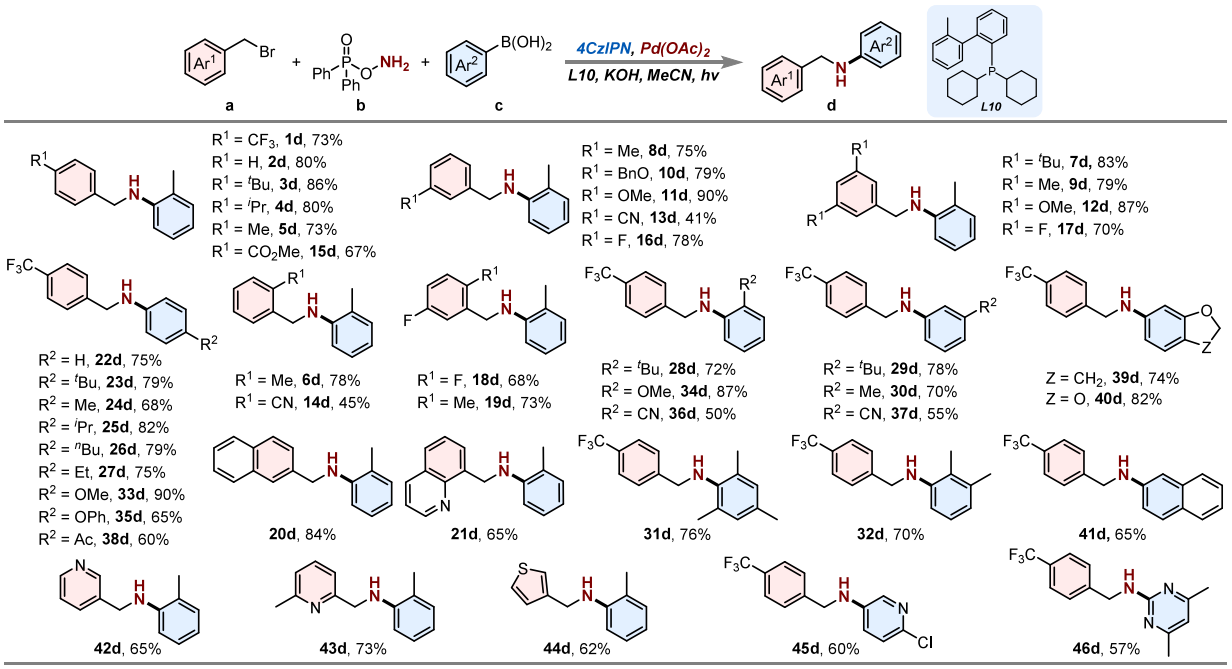

[a]**a** (0.2 mmol), **1b** (0.32 mmol), **c** (0.4 mmol), 4CzIPN (1 mol %), $Pd(OAc)_2$ (9 mol %), **L10** (11 mol %), KOH (2.5 equiv), MeCN, 365 nm, 4.3 W, rt, N_2, and 20 h. [b]Isolated yield.

Scheme 3. Mechanistic Experiments

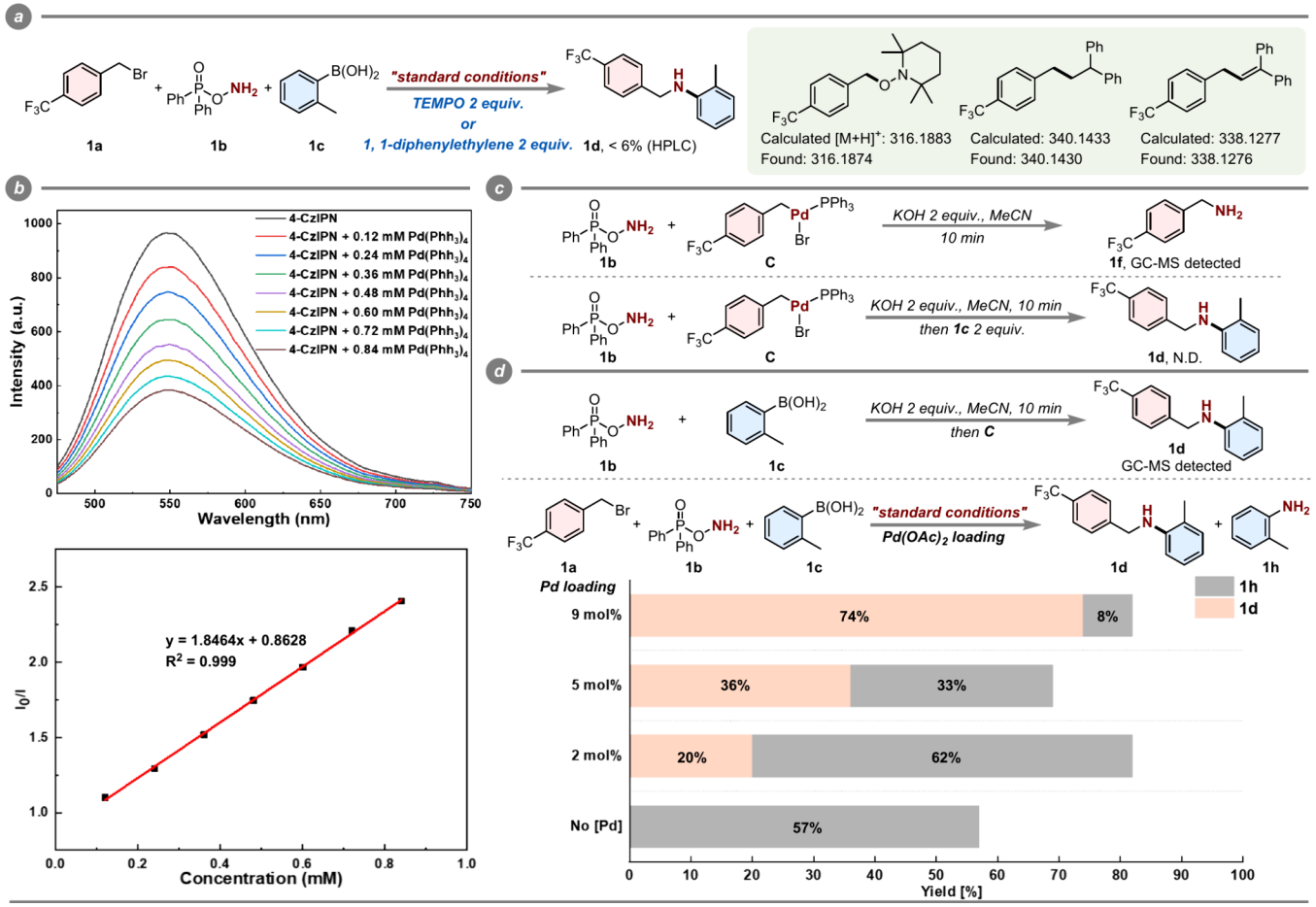

https://doi.org/10.1021/acs.orglett.5c02073
Org. Lett. 2025, 27, 8823−8828

such as pyridine, pyrimidine, and thiophene, were tested, affording 62−65% yields for benzyl bromides (**42d**−**44d**) and 57−60% yields for heteroaryl amines (**45d** and **46d**).

We next gained insight into the catalytic system through controlled experiments. As shown in Table S6, the experimental results show that the integrity of the catalytic system has a decisive influence on the course of the reaction: when the $Pd(OAc)_2$ catalyst was completely absent from the reaction system or, in the meantime, both $Pd(OAc)_2$ and **L10** were missing, the generation of the target product was not observed (entries 2 and 3). Under conditions where only **L10** was absent, the production of a small amount of the target product was detected in 6% yield (entry 4). In the absence of either the base or the photocatalyst 4CzIPN, the reaction proceeded but at a significantly decreased efficiency (entries 5 and 6). Removing **1b** or simultaneously omitting base and photocatalyst halted reactivity (entries 7−9), whereas dark conditions still yielded trace product (entry 10; 6%).

Several mechanism-investigating experiments were then conducted to reveal the photoinduced single-electron pathway. First, radical quenching experiments employing stoichiometric 2,2,6,6-tetramethylpiperidin-1-oxyl (TEMPO) or 1,1-diphenylethylene as radical scavengers in the model system caused sharp yield reductions (Scheme 3a). High-resolution mass spectrometry (HRMS) specifically identified adducts between scavengers and the benzyl radical derived from substrate **1a** (for details, see Figure S7), providing direct evidence of radical propagation. The fluorescence quenching experimental studies were next performed to explore the electron transfer processes. The results showed that Pd^0 exhibited a significant fluorescence quenching effect on excited-state [4CzIPN]*, and the Stern−Volmer curve showed a desirable linear correlation (R^2 = 0.999), as shown in Scheme 3b. When other reaction components were introduced into the system solely, the fluorescence intensity remained essentially unchanged or slightly changed (for details, see Figure S6). The experimental phenomena described above illustrate the existence of a direct SET pathway between [4CzIPN]* and Pd^0 to initiate the catalytic reaction.

We then focused on the C−N−C bond-forming pathway. When a mixture of **1b**, intermediate **C**, and KOH was stirred in MeCN for 10 min, amine **1f** was detected by GC−MS. After the addition of **1c**, however, no desired product was observed, indicating that the reported electrophilic pathway[7] is not operative under our reaction conditions (Scheme 3c). In the nucleophile pathway, arylboronic acid first couples with the aminating reagent to form the C−N bond. Subsequently, a mixture of **1b**, **1c**, and KOH was stirred in MeCN for 10 min. During this stirring, the ^{11}B NMR shift changed from 30.3 ppm (characteristic of **1c**) to 1.7 ppm, indicating N−B bond formation. The addition of intermediate **C** to this mixture then generated desired product **1d**. Without Pd catalysts, only **1h** appears, but higher Pd loadings boost both **1d** and **1h**. Once a threshold is reached, **1d** predominates. These results exhibited that C−N bond formation mainly follows the Pd-promoted arylboronic acid pathway (Scheme 3d; see details in section IV of the Supporting Information).

Based on the above mechanistic experiments and literature reports,[7] the possible reaction paths were presented in Scheme 4. $Pd(OAc)_2$ first forms the **L10**−Pd^0 complex with **L10**. Upon irradiation, 4CzIPN was photoexcited to [4CzIPN]*, which affects a single-electron transfer from **L10**−Pd^0 and oxidizes it to Pd^I complex **A**. Next, $[4CzIPN]^{\bullet -}$ reduces haloarene,

Scheme 4. Proposed Mechanism

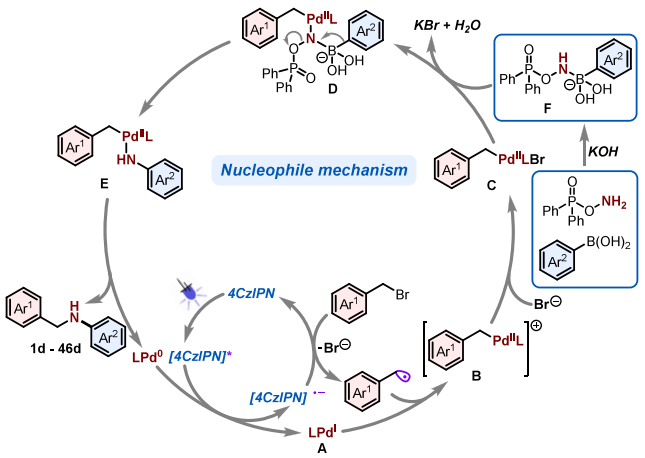

generating $Bn^{\bullet}$ and Br^-. The $Bn^{\bullet}$ radical and the Br^- anion then couple with complex **A** one by one to furnish Pd^{II} complexes **B** and **C**. Later, **1b** and aryl boronic acid engage intermediate **C** under basic conditions to give complex **D**. The metal's Lewis acidity then heightens nitrogen electrophilicity, promoting aryl migration to form complex **E**, which undergoes reductive elimination to deliver the target product.

In summary, we innovatively developed a photocatalytic strategy to integrate a nitrene insertion approach into the Suzuki−Miyaura $C(sp^2)$−$C(sp^3)$ coupling reaction system. Under visible light irradiation, the reaction is successfully reconfigured by the synergistic effect of photocatalyst, palladium catalyst, amination reagent, ligand, and base, and an efficient conversion from conventional $C(sp^2)$−$C(sp^3)$ bond coupling to a $C(sp^2)$−N−$C(sp^3)$ bridging linkage is achieved. High-throughput screening rapidly identifies the optimal combination of reaction parameters. The protocol displays mild conditions, convenient operation, and broad tolerance toward diverse polar functional groups and pharmaceutically relevant heterocycles. The mechanism investigation revealed a single-electron pathway instead of the traditional two-electron processes. Overall, this strategy expands the landscape of cross-coupling chemistry, providing a new avenue for constructing complex $C(sp^2)$−N−$C(sp^3)$ frameworks with significant practical and theoretical implications.

■ ASSOCIATED CONTENT

Data Availability Statement

The data underlying this study are available in the published article and its Supporting Information.

Supporting Information

The Supporting Information is available free of charge at https://pubs.acs.org/doi/10.1021/acs.orglett.5c02073.

Mechanism investigations, synthetic procedures, characterization data, and NMR spectra of these synthesized compounds (PDF)

■ AUTHOR INFORMATION

Corresponding Authors

Yunhe Jin − *State Key Laboratory of Fine Chemicals, Frontier Science Center for Smart Materials, School of Chemistry, Dalian University of Technology, Dalian 116024, China;*

https://doi.org/10.1021/acs.orglett.5c02073
Org. Lett. 2025, 27, 8823−8828

orcid.org/0000-0003-0626-4587; Email: jinyh18@dlut.edu.cn

Shengyang Tao − *State Key Laboratory of Fine Chemicals, Frontier Science Center for Smart Materials, School of Chemistry, Dalian University of Technology, Dalian 116024, China;* orcid.org/0000-0002-0567-8860; Email: taosy@dlut.edu.cn

Authors

Fujun Li − *State Key Laboratory of Fine Chemicals, Frontier Science Center for Smart Materials, School of Chemistry, Dalian University of Technology, Dalian 116024, China;* orcid.org/0009-0009-2888-4841

Yun Zou − *State Key Laboratory of Fine Chemicals, Frontier Science Center for Smart Materials, School of Chemistry, Dalian University of Technology, Dalian 116024, China*

Shuyang Liu − *State Key Laboratory of Fine Chemicals, Frontier Science Center for Smart Materials, School of Chemistry, Dalian University of Technology, Dalian 116024, China;* orcid.org/0009-0001-8246-4970

Yiming Xu − *State Key Laboratory of Fine Chemicals, Frontier Science Center for Smart Materials, School of Chemistry, Dalian University of Technology, Dalian 116024, China*

Complete contact information is available at: https://pubs.acs.org/10.1021/acs.orglett.5c02073

Author Contributions

All authors have given approval to the final version of the manuscript.

Notes

The authors declare no competing financial interest.

■ ACKNOWLEDGMENTS

The authors gratefully acknowledge the support of this research by the National Natural Science Foundation of China (22372025), the Fundamental Research Funds for the Central Universities (DUT22LAB607 and DUT22QN226), the Projects of International Cooperation and Exchanges NSFC−BRFFR (22211530456), and the Natural Science Foundation of Liaoning Province (2024-MSLH-080). The authors acknowledge the reviewers for their great help in improving the quality of this manuscript.

■ REFERENCES

(1) (a) Standley, E. A.; Tasker, S. Z.; Jensen, K. L.; Jamison, T. F. Nickel catalysis: synergy between method development and total synthesis. *Acc. Chem. Res.* **2015**, *48*, 1503−1514. (b) Yin, J. Selected applications of Pd- and Cu-catalyzed carbon−heteroatom cross-coupling reactions in the pharmaceutical industry. In *Applications of Transition Metal Catalysis in Drug Discovery and Development: An Industrial Perspective*; Crawley, M. L., Trost, B. M., Eds.; John Wiley & Sons: Hoboken, NJ, 2012; Chapter 3, pp 97−163, DOI: 10.1002/9781118309872.ch3. (c) Xia, Y.; Qiu, D.; Wang, J. Transition-metal-catalyzed cross-couplings through carbene migratory insertion. *Chem. Rev.* **2017**, *117*, 13810−13889. (d) Bernhardson, D. J.; Hubbell, A. K.; Singer, R. A.; Szpera, R.; Tcyrulnikov, S.; Vicini, A. C.; Allais, C. Recent advances in nonprecious metal catalysis. *Org. Process Res. Dev.* **2024**, *28*, 4240−4263.

(2) (a) Devendar, P.; Qu, R.-Y.; Kang, W.-M.; He, B.; Yang, G.-F. Palladium-catalyzed cross-coupling reactions: A powerful tool for the synthesis of agrochemicals. *J. Agric. Food Chem.* **2018**, *66*, 8914−8934. (b) Omidvar, A. Defective carbon nanocone as an anode material for lithium-ion batteries. *ACS Appl. Energy Mater.* **2020**, *3*, 11463−11469. (c) Quant, M.; Hillers-Bendtsen, A. E.; Ghasemi, S.; Erdelyi, M.; Wang, Z.; Muhammad, L. M.; Kann, N.; Mikkelsen, K. V.; Moth-Poulsen, K. Synthesis, characterization and computational evaluation of bicyclooctadienes towards molecular solar thermal energy storage. *Chem. Sci.* **2022**, *13*, 834−841. (d) Leone, A. K.; Mueller, E. A.; McNeil, A. J. The history of palladium-catalyzed cross-couplings should inspire the future of catalyst-transfer polymerization. *J. Am. Chem. Soc.* **2018**, *140*, 15126−15139. (e) Zhu, J.; Yang, C.; Lu, C.; Zhang, F.; Yuan, Z.; Zhuang, X. Two-dimensional porous polymers: From sandwich-like structure to layered skeleton. *Acc. Chem. Res.* **2018**, *51*, 3191−3202.

(3) (a) Johansson Seechurn, C. C. C.; Kitching, M. O.; Colacot, T. J.; Snieckus, V. Palladium-catalyzed cross-coupling: A historical contextual perspective to the 2010 Nobel Prize. *Angew. Chem., Int. Ed.* **2012**, *51*, 5062−5085. (b) Suzuki, A. Cross-coupling reactions of organoboranes: An easy way to construct C−C bonds (Nobel Lecture). *Angew. Chem., Int. Ed.* **2011**, *50*, 6722−6737. (c) Blakemore, D. Suzuki−Miyaura coupling. In *Synthetic Methods in Drug Discovery*; Blakemore, D. C., Doyle, P. M., Fobian, Y. M., Eds.; The Royal Society of Chemistry: Cambridge, U.K., 2016, Vol. *1*, Chapter 1, pp 1−69, DOI: 10.1039/9781782622086-00001.

(4) Ruiz-Castillo, P.; Buchwald, S. L. Applications of palladium-catalyzed C−N cross-coupling reactions. *Chem. Rev.* **2016**, *116*, 12564−12649.

(5) (a) Weix, D. J. Methods and mechanisms for cross-electrophile coupling of Csp^2 halides with alkyl electrophiles. *Acc. Chem. Res.* **2015**, *48*, 1767−1775. (b) Zheng, P.; Zhou, P.; Wang, D.; Xu, W.; Wang, H.; Xu, T. Dual Ni/photoredox-catalyzed asymmetric cross-coupling to access chiral benzylic boronic esters. *Nat. Commun.* **2021**, *12*, 1646.

(6) (a) Padwa, A.; Gruber, R. Photochemical transformations of small ring carbonyl compounds. XVIII. Deuterium isotope effects in the photochemistry of an azetidine ketone. *J. Am. Chem. Soc.* **1968**, *90*, 4456−4458. (b) Dherange, B. D.; Kelly, P. Q.; Liles, J. P.; Sigman, M. S.; Levin, M. D. Carbon atom insertion into pyrroles and indoles promoted by chlorodiazirines. *J. Am. Chem. Soc.* **2021**, *143*, 11337−11344. (c) Lyu, H.; Kevlishvili, I.; Yu, X.; Liu, P.; Dong, G.-B. Boron insertion into alkyl ether bonds via zinc/nickel tandem catalysis. *Science* **2021**, *372*, 175−182. (d) Jurczyk, J.; Woo, J.; Kim, S. F.; Dherange, B. D.; Sarpong, R.; Levin, M. D. Single-atom logic for heterocycle editing. *Nat. Synth.* **2022**, *1*, 352−364.

(7) Onnuch, P.; Ramagonolla, K.; Liu, R. Y. Aminative Suzuki−Miyaura coupling. *Science* **2024**, *383*, 1019−1024.

(8) (a) Kambe, N.; Iwasaki, T.; Terao, J. Pd-catalyzed cross-coupling reactions of alkyl halides. *Chem. Soc. Rev.* **2011**, *40*, 4937−4947. (b) Jana, R.; Pathak, T. P.; Sigman, M. S. Advances in transition metal (Pd, Ni, Fe)-catalyzed cross-coupling reactions using alkyl-organometallics as reaction partners. *Chem. Rev.* **2011**, *111*, 1417−1492. (c) Netherton, M. R.; Fu, G. C. Suzuki cross-couplings of alkyl tosylates that possess β-hydrogen atoms: Synthetic and mechanistic studies. *Angew. Chem., Int. Ed.* **2002**, *41*, 3910−3912. (d) Zhou, Y.; Qiu, L.; Li, J.; Xie, W. A general copper catalytic system for Suzuki−Miyaura cross-coupling of unactivated secondary and primary alkyl halides with arylborons. *J. Am. Chem. Soc.* **2023**, *145*, 28146−28155. (e) Liu, D.; Xiao, F.; Ebel, B.; Oppel, I. M.; Patureau, F. W. Visible-light-mediated radical α-C(sp^3)−H *gem*-difluoroallylation of amides with trifluoromethyl alkenes via halogen atom transfer and 1,5-hydrogen atom transfer. *Org. Lett.* **2025**, *27*, 2377−2382.

(9) (a) Stephenson, C.; Yoon, T.; MacMillan, D. W. C. *Visible Light Photocatalysis in Organic Chemistry*; John Wiley & Sons: Hoboken, NJ, 2018; DOI: 10.1002/9783527674145. (b) Luo, J.; Zhang, J. Donor-acceptor fluorophores for visible-light-promoted organic synthesis: photoredox/Ni dual catalytic C(sp^3)−C(sp^2) cross-coupling. *ACS Catal.* **2016**, *6*, 873−877.

(10) Skubi, K. L.; Blum, T. R.; Yoon, T. P. Dual catalysis strategies in photochemical synthesis. *Chem. Rev.* **2016**, *116*, 10035−10074.

(11) Tellis, J. C.; Primer, D. N.; Molander, G. A. Single-electron transmetalation in organoboron cross-coupling by photoredox/Ni dual catalysis. *Science* **2014**, *345*, 433−436.

(12) (a) Luo, J.; Zhang, J. Donor-acceptor fluorophores for visible-light-promoted organic synthesis: photoredox/Ni dual catalytic $C(sp^3)-C(sp^2)$ cross-coupling. *ACS Catal.* **2016**, *6*, 873−877. (b) Kuo, T.-C.; Malvadkar, N. A.; Drumright, R.; Cesaretti, R.; Bishop, M. T. High-throughput industrial coatings research at The Dow Chemical Company. *ACS Comb. Sci.* **2016**, *18*, 507−526.

(13) (a) Zhang, Y.; Fu, D.; Chen, Z.; Cui, R.; He, W.; Wang, H.; Chen, J.; Chen, Y.; Li, S.-J.; Lan, Y.; Duan, C.; Jin, Y. Bifunctional iron-catalyzed alkyne *Z*-selective hydroalkylation and tandem *Z*−*E* inversion via radical molding and flipping. *Nat. Commun.* **2024**, *15*, 8619. (b) Liu, S.; Gan, Z.; Jiang, M.; Liao, Q.; Lu, Y.; Wang, H.; Xue, Z.; Chen, Z.; Zhang, Y.; Yang, X.; Duan, C.; Jin, Y. Selective arene photonitration *via* iron-complex *β*-homolysis. *JACS Au* **2024**, *4*, 4899−4909. (c) Liu, S.; Lu, Y.; Wang, H.; Xue, Z.; Xu, Z.; Wan, H.; Yin, Q.; Lv, T.; Liu, S.-X.; Jin, Y. Iron-catalyzed *ipso*-nitration of aryl borides *via* visible-light-induced *β*-homolysis. *ACS Catal.* **2025**, *15*, 3306−3313.

https://doi.org/10.1021/acs.orglett.5c02073
Org. Lett. 2025, 27, 8823−8828